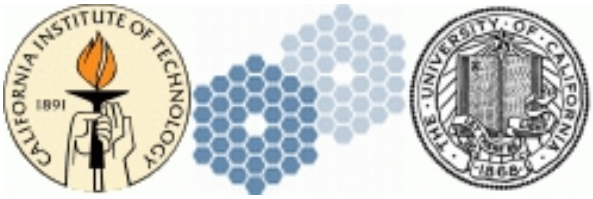

AO Photometry for NGAO
Keck Adaptive Optics Note 474

Matthew Britton, COO
Richard Dekany, COO
Ralf Flicker, WMKO
Claire Max, UCSC
Chris Neyman, WMKO
Knut Olsen, NOAO

April 10, 2007

1 Introduction

Photometry in adaptive optics constitutes an intricate and multifaceted problem. The issue touches on a wide range of astronomical topics, in which one is interested in performing differential or absolute photometry on point sources or resolved objects. The astronomical targets may be as simple as well separated binary star system, or may be much more complex, involving crowded stellar fields with a wide range of stellar magnitudes and overlapping point spread functions (PSFs). For observations of resolved objects such as planets and galaxies, the finite angular extent of the PSF causes distinct features to blur, raising the issue of the effective dynamic range that one may achieve. In a number of applications involving resolved objects, point sources are embedded in an extended emission region and it is of interest to isolate their photometric contribution from the background emission.

Photometric applications may employ imagers with broadband or narrowband filters, slit spectrographs, or integral field unit spectrographs. Each of these types of instrumentation introduces its own set of considerations in extracting photometry from the pixel data read out from the detector. The detectors themselves introduce a number of effects that impact the photometric precision one may achieve on a particular target. These include nonlinear pixel response arising from finite detector well depth, spurious signals induced by cosmic rays, flat fielding errors, and the presence of dark current and read noise. These effects vary in relative importance and net impact on photometric accuracy, depending on the character of the observation and the level of effort expended on calibration.

There are two broad approaches to photometric data analysis. In situations where objects of interest are well-separated, aperture photometry provides a straightforward approach. For more complex fields in which one wishes to perform photometry on crowded stellar fields or resolved objects whose point spread functions overlap, one must resort to deconvolution algorithms to separate the contributions from different objects. For applications involving integral field unit spectroscopy, these considerations must be extended to include extraction of spatially resolved spectra from the three dimensional data cube.

Each of the above considerations is familiar from astronomical experience with seeing limited instrumentation, and issues related to photometric precision are not a novelty raised by adaptive optics. However, adaptive optics systems introduce a host of new effects that can impact photometric accuracy. These effects arise from the way in which these systems respond to atmospheric turbulence, and from the resulting profound change in the PSF in moving from the seeing limit towards the diffraction limit. A qualitative introduction to these effects is presented in the next section.

2 Photometry in Adaptive Optics

Adaptive optics (AO) systems potentially offer significant advantages for photometric applications, but realization of this potential is complicated by a number of different effects.

A clear advantage delivered by adaptive optics is the diffraction limited resolution that results from atmospheric turbulence compensation. An adaptive optics system delivers a fraction of the total light in a diffraction limited core that is typically an order of magnitude narrower than the seeing limited PSF. This core provides a significant benefit for targets that suffer from confusion when observed in the seeing limit, and a substantial improvement in the sensitivity of the observation. The balance of light is scattered into a broad, seeing limited halo surrounding the core. The relative proportion of light in the core and halo varies with the quality of adaptive correction. One's ability to separate

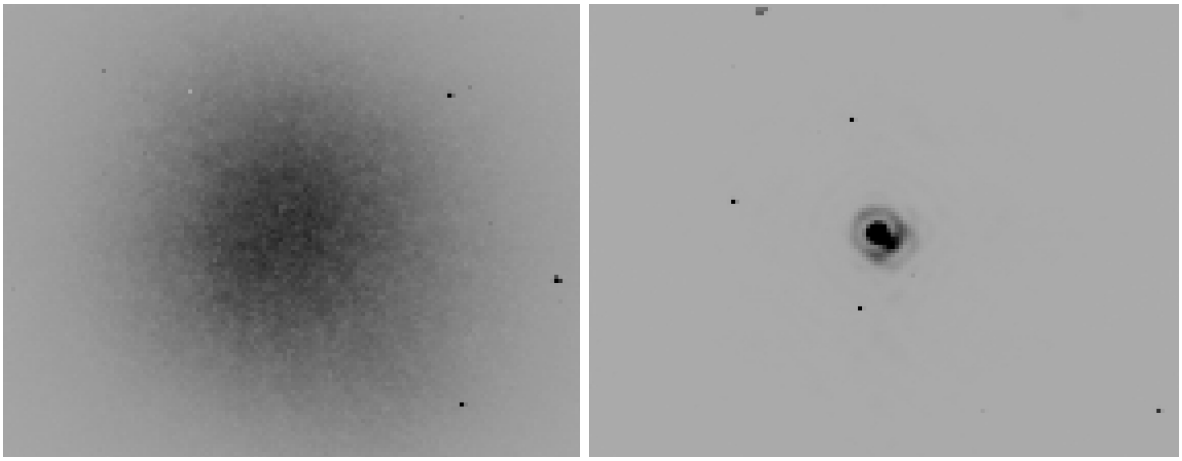

Figure 1: Illustrative example of photometric issues arising in observations of a close binary. A seeing limited observation appears at left, in which there is no hope of separating the photometric contribution from each member of the binary. An adaptive optics observation appears at right, illustrating that the diffraction limited cores of the binary members have been resolved. Despite this, performing differential photometry on this binary pair remains a challenge due to the fact that the point spread functions overlap. In this circumstance aperture photometry is unsuitable. Direct deconvolution is possible if an estimate of the PSF is available. Without such an estimate, one must resort to blind deconvolution methods. It should be noted that for this K band observation, the Strehl ratio was of order 50%, so that a significant fraction of light remains in a halo surrounding each star. This halo is not apparent at the stretch shown in the image.

the photometric contributions from objects at small angular separations can depend quite strongly on the proportion of light in the core. For example, consider the AO compensated image in Figure 1. The stars may be readily resolved by eye in the image data, but accurate photometry will still be a challenge due to the fact that the light in the halo of one star is blended with light in the Airy ring of the other. The importance of this effect depends strongly on the stability and quality of AO compensation, the angular separation and differential magnitude, and the required level of photometric precision.

A significant complication arising in adaptive optics is that the PSF delivered by such a system displays far more variability than the seeing limited PSF. The AO PSF varies significantly in time, over the field of view, and in wavelength. This strong variability is the single aspect of adaptive optics observations that poses a signficantly greater challenge to photometric data reduction when compared to seeing limited observations. Here we

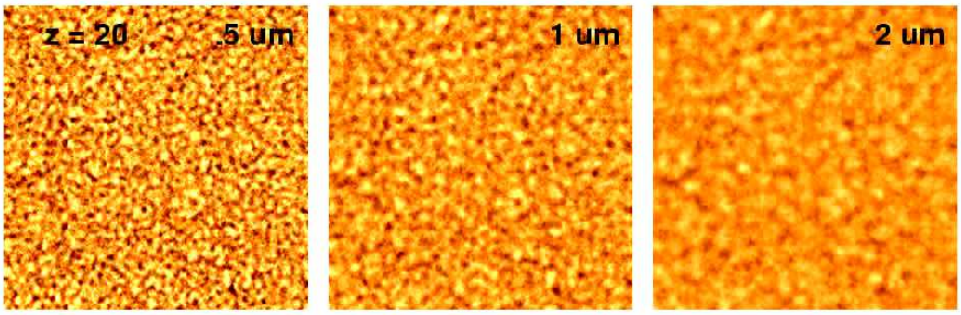

Figure 2: Simulation of wavefront amplitude fluctuations in the pupil plane of a telescope arising from scintillation. The panels shows amplitude fluctuations across a 5 meter patch of wavefront that arise from traversing a turbulence screen and propagating twenty kilometers. The Fried parameter of the screen used in this simulation was 65 cm at .5 μm. The three panels display an increase in the lateral coherence scale and a decrease in the strength of the amplitude fluctuations as one shifts from .5 μm to 2 μm observing wavelengths.

present a qualitative description of this PSF variability.

An adaptive optics system aims to compensate for wavefront phase aberrations arising from atmospheric turbulence. These phase aberrations arise from fluctuations in the index of refraction of air above the telescope, which themselves arise in a turbulent cascade induced by weather and geographical features. As the wind carries the turbulent air over the telescope, the phase errors in the wavefront arriving at the telescope evolve rapidly in time. The adaptive optics system compensates for these variations on timescales of order a millisecond. Residual, uncorrected wavefront phase errors that cannot be compensated by the AO system will evolve on this same timescale, and these phase errors will scatter light out of the PSF core. For astronomical applications, integration times are almost always much longer than this millisecond timescale, so that the scattered light is averaged into a broad halo. For this reason, the adaptive optics PSF displays a core/halo morphology.

A second, subtler effect that occurs as wave propagate through atmospheric turbulence is scintillation. This effect arises from phase aberrations induced by higher altitude turbulence, which are converted through free space propagation to amplitude fluctuations in the pupil plane of the telescope. A simulation of the effects of scintillation on the wavefront amplitude is shown in Figure 2. These random amplitude fluctuations lead to flucutuations in the total intensity of the PSF, which may be problematic in applications requiring extremely precise photometry.

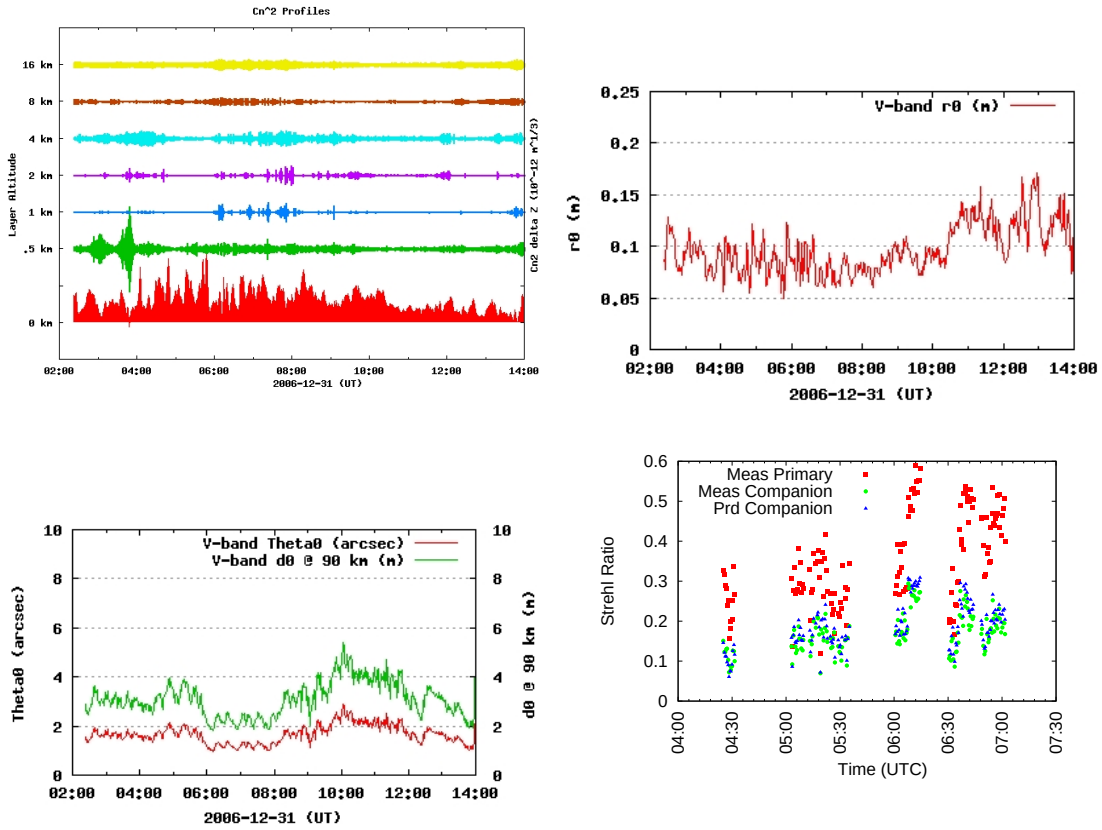

Figure 3: Turbulence profiles and their effect on astronomical observations. The upper left panel shows the evolution of the C_n^2 profile over a single night at Palomar observatory, as measured by a DIMM/MASS instrument. This instrument yields a measure of $C_n^2 \Delta z$ at each of 7 altitudes once a minute. The strength of turbulence is proportional to the height of the line in the plot. The upper right panel shows the Fried parameter r_0 computed from these profiles, while the lower left panel shows the isoplanatic angle θ_0 and focal anisoplanatism parameter d_0 computed from these turbulence profiles. Considerable temporal variability is apparent in the turbulence profiles, and in each of these turbulence parameters. This gives rise to evolution in the point spread function delivered by the adaptive optics system. As an illustration of this effect, observed Strehl ratios for a 20 asec binary system are plotted as a function of time in the lower right panel. The guide star Strehl ratios evolve with the turbulence and wind profiles. The companion Strehl ratio evolves due to these effects and due to anisoplanatism.

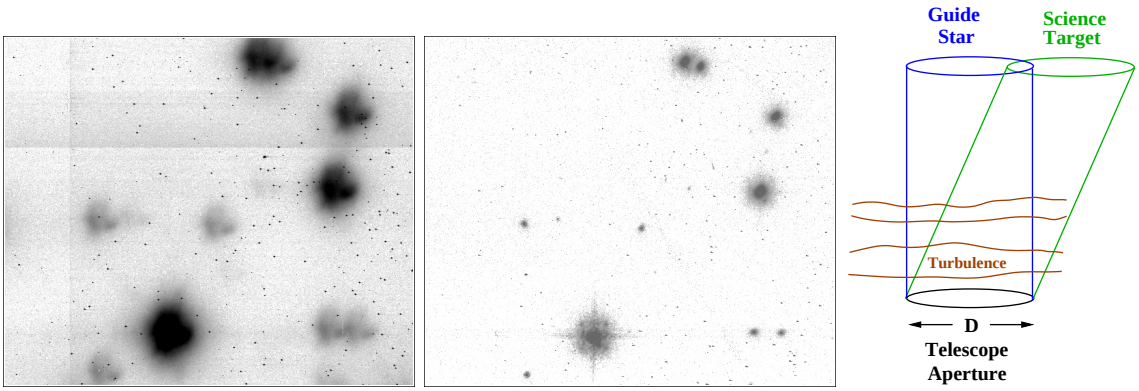

Figure 4: Seeing limited and adaptive optics compensated images of the Trapezium cluster. At left is shown a 30 sec. K band image of the Trapezium cluster taken in the seeing limit. The deleterious effects of atmospheric turbulence are clearly apparent. The center panel shows the same field after compensation by an adaptive optics system. The guide star appears at the bottom edge of the image. The PSF delivered by the adaptive optics system degrades with increasing angular offset from the guide star due to anisoplanatism. This effect appears in this image as a radial elongation of the PSF that increases with angular offset from the guide star. Anisoplanatism arises from the shear between the column of turbulence traversed by the guide star and that traversed by a target at finite angular offset, as pictured in the right panel. The adaptive optics system acts to compensate wavefront errors of the guide star, and this compensation decorrelates with increasing angular offset from the guide star.

On timescales of order minutes to hours, the statistical properties of atmospheric turbulence evolve. An illustration is shown in Figure 3, which displays the vertical distribution of atmospheric turbulence as a function of time for a single night at Palomar Observatory. At random times throughout the night, bursts of turbulence occur at various altitudes, and last for timescales of order 10 minutes. This temporal evolution of the turbulence profile gives rise to evolution in familiar measures of atmospheric turbulence, such as the Fried parameter r_0, isoplanatic angle θ_0 and focal anisoplanatism parameter d_0. Similarly, the vertical wind profile (i.e. wind speed and direction as a function of altitude) can evolve on timescales of hours due to local weather patterns. This wind profile will affect the timescale on which wavefront phase errors evolve.

The temporal dependence of atmospheric turbulence and wind profiles play a very large role in the evolution of the PSF delivered by an adaptive optics system. The ability of the AO system to compensate for wavefront phase errors depends on a host of considerations,

including the update rate and control laws used in driving the adaptive mirrors, the actuator count on the adaptive mirror, and the brightness of the guide star used to sense the wavefront aberrations. These effects each act to degrade the PSF delivered by the adaptive optics system. As the statistical properties of atmospheric turbulence evolve in time, these effects change in relative importance, modifying the PSF delivered by the adaptive optics system. An illustration of this behavior is shown in Figure 3, which displays temporal evolution in the measured Strehl ratios of two PSFs extracted from observations of a binary system.

Unlike the seeing limited PSF, the PSF of a classical single conjugate adaptive optics system varies over the field due to residual wavefront errors from atmospheric turbulence. This effect arises from the fact that the adaptive optics system aims to stabilize the wavefront of the guide star. Wavefronts from sources at finite angular offset traverse a different column of atmospheric turbulence due to the shearing of the beams, as shown in Figure 4. This effect is known as anisoplanatism, and leads to degradation of the PSF as the angular offset from the guide star increases. As the statistical properties of atmospheric turbulence evolve in time, the effects of anisoplanatism cause the PSF to change in both time and field position, leading to a complex evolution of the image quality. Advanced AO architectures such as multiconjugate AO (MCAO) and multiobject AO (MOAO) aim to mitigate the effects of field dependent PSF evolution by performing compensation using multiple adaptive mirrors. The level of PSF stability over the field that these systems will be able to deliver is currently an active topic of research and development in adaptive optics. However, as in single conjugate AO systems there will be significant temporal evolution in the PSF, as the performance delivered by these systems will evolve in response to the changing turbulence profile.

Morphological features in the PSF are induced by telescope optics and optical misalignments. Diffraction from spiders and from the central obscuration are readily apparent in adaptive optics image data, such as those shown in Figure 4. Calibration errors in the optical system can likewise lead to persistent features in the PSF. These features may evolve as the telescope and instrumentation are subjected to changing gravity load. Finally, field dependent optical aberrations can affect the PSF as well. These effects are present in the seeing limited observations, but are far more pronounced in adaptive optics observations that deliver diffraction limited PSFs. The image data in Figure 4 are illustrative, in that the diffraction pattern from spiders apparent in the AO compensated images are blurred away in the seeing limited images.

Finally, the seeing limited PSF displays a very weak wavelength dependence. The FWHM of the PSF scales as $\lambda^{-1/5}$. In contrast, the width of the diffraction limited PSF scales as λ, and many of the error terms in adaptive optics scale as $\lambda^{6/5}$. This steeper dependence leads to pronounced wavelength evolution in the morphology of the PSF

delivered by the adaptive optics system, which shifts light from the core to the halo as the observing wavelength decreases.

To summarize, the temporal evolution of the atmospheric turbulence profile and the wind velocity profile generate a number of effects that modify the morphology of the adaptive optics PSF in time, field location, and wavelength. Additional static and time dependent effects can arise from static or quasistatic effects in the telescope and instrument optics. Some of these effects are present in seeing limited observations, but become much more apparent in the diffraction limited PSF delivered by the adaptive optics system. Others, such as wavelength dependence, display a much more pronounced effect on the adaptive optics PSF. Still others, such as anisoplanatism, have no seeing limited analogue. The consequence of these dependencies is to introduce substantial variability in the PSF delivered by the AO system. This variability can significantly complicate the photometric analysis of adaptive optics data, as it changes the proportion of light in the core and halo of the PSF. This leads to variability in the blending of PSFs in observations like the one shown in Figure 1. This situation has proved a significant impediment to the application of deconvolution algorithms used for photometric data reduction. To date, such algorithms have been hard pressed to account for the variations in the AO PSF while remaining computationally tractable enough to accomodate realistic data sets.

3 Astronomical Applications

In this section we will briefly review some astronomical applications of recent interest that require accurate photometry or high dynamic range imaging and spectroscopy.

3.1 Planetary Astronomy

Adaptive optics observations of objects within our solar system constitute a significant fraction of photometric applications. The objects targeted by these studies are often resolved by the telescope, and deconvolution algorithms are commonly applied to measure the surface features. Deconvolution has been carried out using PSF reference stars. Myopic deconvolution algorithms are also widely employed in these studies. This type of deconvolution aims to extract both the point spread function and the brightness distribution of the object from a series of images.

Near infrared adaptive optics observations of Io have been conducted at Keck Observatory [1]. The images display strong, pointlike emission features from volcanoes on the surface of this moon, along with diffuse emission from the planetary surface. Among other goals, these observations aimed to measure blackbody temperatures of the volcanic

regions, and deconvolution algorithms were employed to identify flux from the individual volcanoes. Observations were acquired using both Io and Ganymede as guide objects for the adaptive optics system. The latter source served as the guide object when Io was in Jupiter's shadow, which suppressed reflected light from the planetary surface. The angular separation between Ganymede and Io was 30 asec in this experiment, and anisoplanatism introduced significant PSF degradation when guiding on the former source.

Near infrared adaptive optics observations of Uranus have been conducted at Keck Observatory[2] to measure photometry of satellites and rings. Photometry of satellites was measured using aperture photometry techniques, which were not possible to apply when scattered light from the planet overwhelmed the satellites near periapse. Ring brightnesses were determined using a constrained model of the ring/planet system and an AO PSF measured from a calibration star.

Near infrared adaptive optics observations of Titan have been conducted at Keck Observatory[3] to measure the surface photometry. This study used myopic deconvolution techniques to analyze the image data, and identified asymmetries in the surface brightness of the planet.

Photometric observations of asteroids have been performed with adaptive optics systems. Recent results include near infrared imaging and spectroscopy of Vesta [4] and imaging of a number of main-belt asteroids [5] using the Keck adaptive optics system. These studies utilized myopic deconvolution algorithms to study size, binarity, and surface brightness features of these asteroids.

3.2 Stellar Photometry

Photometric observations of crowded stellar fields is a natural application for adaptive optics, as the diffraction limited core ignificantly reduces confusion present in seeing limited observations. However, significant challenges remain due to PSF variability, particularly that arising from anisoplanatism.

Near infrared observations of the Galactic Center were conducted with the laser guide star adaptive optics system at Keck Observatory to measure photometric variability of Sagittarius A*[6]. These observations employed a point source deconvolution method to identify and subtract away the point spread functions of stars near Sag A*, and then performed aperture photometry on the extended emission region to determine the flux of this object.

The advantages of adaptive optics may be significant for a variety of applications currently pursued with seeing limited instrumentation. Searches and monitoring of variable stars in crowded fields have been conducted in the seeing limit[7]. Crowded fields are often chosen in variable star surveys to increase the detection rate, and followup observations

with an adaptive optics system have the potential to improve the photometric accuracy of the observed light curves. Recent interest in this area has focused on the photometric detection of eclipsing planets [8, 9] and microlensing events[10]. Note that the latter application in particular requires followup AO observations be conducted in response to alert events generated by survey programs.

Differential photometry of binary and multiple star systems constitutes a well-defined problem in adaptive optics, and a number of studies have aimed to establish the photometric precision that may be achieved from such data. Unsurprisingly, the most accurate results have been obtained in cases for which the stars were far enough apart that there was no overlap among the PSFs. Roberts *et al.*[11] performed IJHK band observations using the 3.6m AEOS telescope. This study measured differential photometry stable to 1 part in 10^2 for binaries up to 5 asec in separation. Britton[12] performed narrowband near-IR observations of a 20 asec binary at 1.65 and 2.12 μm on the Hale 5m at Palomar Observatory and measured differential photometry to 1 part in 10^3. Christou & Drummond[13] performed adaptive optics observations using the Shane 3m telescope at Lick Observatory. This study obtained differential photometric accuracies of order a few parts in 10^2 for systems with separations up to 12 asec. Differential photometry of order .1 mag has been obtained in the Galactic Center, where confusion arises from the blending of PSFs from adjacent stars[14].

3.3 Extragalactic Science

Spatially resolved spectroscopy of extragalactic targets is an area of research that is becoming a strong driver for AO development. In these applications, moderate resolution spectra may be used to map the composition, star formation history, and internal dynamics of galaxies over a wide range of redshifts[15]. These applications call for integral field unit observations of faint galaxies, and require an angular resolution of order 100 mas. The high sensitivity and high angular resolution afforded by adaptive optics constitute a fatally attractive combination that may be brought to bear on this problem. At present the first indications of these types of observations are available through seeing limited and AO compensated IFU spectrographs and image data.

Imaging observations of galaxies have been acquired using the Keck laser guide star adaptive optics system under the CfAO Treasury Survey project [16, 17]. This project aims to image galaxies observed as part of the Great Space Observatories program. The morphologies of these galaxies are resolved using adaptive optics, and accurate photometry is required to probe the star formation history. These observations were reduced using field dependent PSF estimates derived from observations of dense stellar clusters obtained before or after the science exposures.

Imaging observations of field galaxies have been performed using the NAOS natural guide star adaptive optics system and the CONICA IR camera at the VLT [18, 19]. These observations were reduced using field dependent PSF estimates derived from stars within the science frames, coupled with semianalytic models used to interpolate to the locations of the galaxies.

Integral field unit spectroscopy of a z=1.5 galaxy has been carried out using the OSIRIS integral field unit spectrograph fed by the laser guide star adaptive optics system at Keck Observatory[20]. The laser beacon was pointed directly at the science target, while a star 55 asec away from the science target was used for tip tilt guiding. The observed object was very faint ($m_H \approx 23$), and the analysis did not attempt to extract precise photometry.

4 Effects on Photometry

A large number of effects can influence the accuracy of photometric measurements. This section describes a number of these effects, with particular emphasis on those that are associated with adaptive optics systems.

4.1 Atmospheric Turbulence Effects

4.1.1 PSF Evolution

As discussed in the introduction, the PSF of a single conjugate adaptive optics system varies in time, field location, and wavelength in response to temporal evolution of the turbulence and wind profiles. A model that captures the functional dependencies of the PSF on these parameters can be extremely useful in identifying and understanding the implications of PSF evolution. Such a model has been developed to describe the field dependent, long exposure optical transfer function (OTF) delivered by a single conjugate adaptive optics system[21, 12], from which the PSF may be obtained via Fourier transformation. Using the notation in the latter paper, the field dependent, long exposure OTF delivered by a natural guide star adaptive optics system may be written in terms of the long exposure guide star optical transfer function $OTF_{\rm gs}(\mathbf{r})$ as

$$OTF(\vec{r}) = \exp\left[-\frac{1}{2}D_{\rm apl}(\vec{r})\right] OTF_{\rm gs}(\vec{r}) \tag{1}$$

Here $\vec{r}$ is a vector in the pupil plane of the telescope, and the quantity $D_{\rm apl}(\vec{r})$ is the anisoplanatic structure function, which accounts for the field dependent degradation that

arises from anisoplanatism. This structure function takes the form

$$D_{\text{apl}}\left(\vec{r}\right) = 2^{8/3}\Xi k^2 \int_0^\infty dz\; C_n^2(z) \left\{ 2\left|z\vec{\theta}\right|^{5/3} + 2\left|\vec{r}\right|^{5/3} - \left|\vec{r} + z\vec{\theta}\right|^{5/3} - \left|\vec{r} - z\vec{\theta}\right|^{5/3} \right\} \quad (2)$$

In this equation for $D_{\text{apl}}\left(\vec{r}\right)$, k is the wavenumber, $C_n^2(z)$ is the turbulence profile along the line of sight to the guide star, z is the range variable, $\vec{\theta}$ is the angular offset between the guide star and the point of interest in the field, and the constant Ξ=.458986. This equation explicitly captures the field dependence of the anisoplanatic structure function through the variable $\vec{\theta}$, the wavelength dependence through k, and the dependence on turbulence profile through the quantity $C_n^2(z)$. Dependence on the telescope aperture diameter arises implicitly through $\vec{r}$, and zenith angle dependence is captured in the range variable z and the turbulence profile $C_n^2(z)$. Time dependence of $D_{\text{apl}}\left(\vec{r}\right)$ enters through the turbulence profile, as indicated in Figure 3. Additional time dependence arises from the change in zenith angle that occurs as the telescope tracks a target. In addition to these dependencies, the model in Equation 1 encapsulates the complex response of the adaptive optics system to evolution in the turbulence and wind profiles through the guide star optical transfer function $OTF_{gs}(\vec{r})$.

The model in Equation 1 is applicable to natural guide star adaptive optics observations, and extending this model to laser guide star observations is desirable. For these observations, additional dependencies arise from the height of the beacon and the location of the tilt guide star with respect to the laser. In addition, the factorization of the optical transfer function into an anisoplanatic component and $OTF_{gs}(\vec{r})$ that occurs for a natural guide star AO observation is no longer valid for laser guide stars. This unfortunate complication arises from the effects of focal anisoplanatism, which act to break the pupil plane symmetry that occurs in the NGS case. Research is currently underway to extend this model to laser guide star adaptive optics observations.

The above considerations hold for single conjugate adaptive optics architectures, in which anisoplanatism is an unavoidable consequence of the single deformable mirror. Advanced adaptive optics architectures currently under consideration for NGAO utilize multiple deformable mirrors, and can act to eliminate the field dependence of the point spread function delivered by the adaptive optics system. Multiconjugate AO (MCAO) systems aim to eliminate the field dependence of the PSF using multiple deformable mirrors placed at different optical conjugates. The conjugation of these mirrors to multiple altitudes acts to mimic the vertical distribution of atmospheric turbulence within the optical system. This permits these systems to compensate for shearing among beams from different targets in the field, thereby eliminating the effects of anisoplanatism. These systems require multiple guide stars in order to sense the three dimensional volume of

atmospheric turbulence above the telescope. The first astronomical MCAO system scheduled for deployment is the VLT Multiconjugate Adaptive Optics Demonstrator (MAD). This system will be followed by the facility class Gemini South MCAO system, which uses three deformable mirrors and five sodium laser guide stars. This system is scheduled to be deployed in about a year.

Multiobject AO (MOAO) systems aim to provide independent AO compensation for each of a number of subfields within a larger field of view. This architecture also utilizes multiple guide stars to sense the three dimensional volume of atmospheric turbulence. However, in this architecture there is an independent deformable mirror for each science target, which acts to provide an independent correction specific to its line of sight through the atmosphere. In this way, the architecture delivers a point spread function that does not suffer from anisoplanatism. One advantage of MOAO over MCAO is that these independent deformable mirrors can permit MOAO compensation over fields of view wider than that afforded by MCAO. However, MOAO is an astronomical adaptive optics architecture that has only recently been proposed, and the stability of the PSF delivered by such a system is an open question.

It is important to emphasize that time dependence of the PSF delivered by MCAO and MOAO systems will still occur due to temporal evolution in the turbulence and wind profiles and the resulting evolution in the response of the adaptive optics system. Likewise, evolution in the zenith angle as the telescope tracks the astronomical target will induce variation in the delivered PSF. Given the complexity of these advanced adaptive optics architectures, the temporal evolution may be expected to be at least as severe as that delivered by a single conjugate system. The issues of photometric precision that may be obtained with these systems is an open topic. This will likely remain the case until one of these advanced architectures sees first light.

4.1.2 Scintillation

Scintillation arises when a wavefront in which phase aberrations are present propagates through space. The propagation converts the wavefront phase aberrations into amplitude aberrations, as shown in Figure 2. This effect can lead to photometric fluctuations of order 1 millimagnitude[22].

The expression for the log amplitude variance of a plane wave propagating through turbulence is

$$\sigma_\chi^2 = .5631 k_0^{7/6} \mu_{5/6} \tag{3}$$

Here k_0 is the wavenumber and the turbulence moment $\mu_{5/6}$ is defined as

$$\mu_m = \int_0^\infty dz\ C_n^2(z)\ z^m \tag{4}$$

Under typical turbulence conditions at Palomar, one finds a value of $\mu_{5/6} = 2.6 \times 10^{-10}$ m$^{3/2}$ at zenith.

The variance in the intensity is related to the log amplitude variance by

$$\frac{\sigma_I^2}{I^2} = 4\sigma_\chi^2 \tag{5}$$

Thus, the fractional variance of the intensity is four times the log amplitude variance, and the fractional standard deviation of the intensity is twice the standard deviation of the log amplitude. Figure 5 shows σ_I/I vs. wavelength at zenith under typical turbulence conditions at Palomar.

The intensity fluctuations in the pupil plane display a lateral coherence scale that depends on turbulence conditions and observing wavelength, as indicated in Figure 2. This coherence scale is an important parameter in determining how the effects of scintillation average away in time and over finite apertures.

An expression for the aperture averaged log amplitude variance has been derived for the case in which the aperture is much larger than this coherence scale. The expression is

$$\sigma_{\chi A}^2 = 4.34 \frac{\mu_2}{D^{7/3}} \tag{6}$$

where D is the aperture diameter. Under typical turbulence conditions at Palomar, one finds a value of $\mu_2 = 1.1 \times 10^{-5}$ m$^{8/3}$ at zenith. Note that the wavelength dependence drops out of $\sigma_{\chi A}^2$.

One can form a ratio between the non-aperture averaged log amplitude variance and the aperture averaged log amplitude variance as

$$\frac{\sigma_{\chi A}^2}{\sigma_\chi^2} = \left(\frac{D_c}{D}\right)^{7/3} \quad D \gg D_c \tag{7}$$

where

$$D_c = .957\sqrt{\lambda}\left(\frac{\mu_2}{\mu_{5/6}}\right)^{3/7} \tag{8}$$

is the characteristic lateral coherence scale. The above ratio illustrates the degree of suppression that arises from aperture averaging. Figure 6 displays the characteristic lateral coherence scale and the ratio described above.

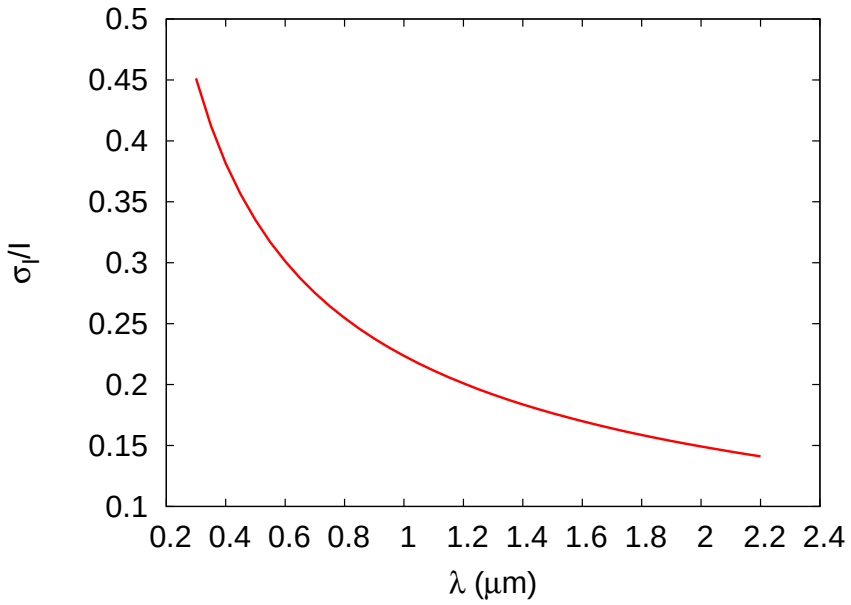

Figure 5: Fractional standard deviation of intensity in the telescope pupil plane as a function of wavelength for typical turbulence conditions at Palomar. Plane wave propagation through turbulence gives rise to the effect of scintillation, which generates fluctuations in the wave amplitude at the pupil plane of the telescope. The fractional fluctuation in the pupil plane intensity is plotted above.

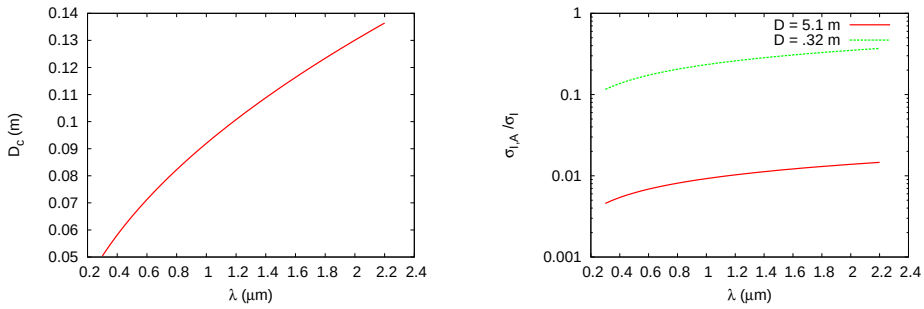

Figure 6: Plots of the lateral coherence scale and the fractional suppression of scintillation arising from aperture averaging. The left plot shows the lateral coherence scale as a function of wavelength. This parameter increases as $\sqrt{\lambda}$. The right plot shows the fraction by which the intensity fluctuations are suppressed due to averaging over a 5.1 and .32 m apertures.

The implications of this analysis for high precision photometry are quite straightforward. Using equation 6, one finds that for a 5.1 meter aperture, the standard deviation of the aperture averaged intensity is .2%. This does not mean that the entire point spread function on the Hale 5m telescope is varying by .2%. Instead, it means that there is a significant amount of variation in the PSF at a radius corresponding to the characteristic lateral coherence scale, which when averaged over the entire PSF leads to a .2% fluctuation in intensity. The radius corresponding to the lateral coherence scale is plotted in Figure 7. This variance will decrease with integration time, and for typical astronomical integration times the photometric variability arising from scintillation should be under a millimagnitude.

4.2 Atmospheric Attenuation

Effects such as molecular absorption, Rayleigh scattering, and aerosol scattering act to attenuate light from astronomical targets. This atmospheric attenuation reduces the observed flux in a way that depends on the altitude of the observatory, the zenith angle of the observation, and the wavelength of the radiation. In addition to this simple correction, temporal variability in the atmosphere arises from variability in the scattering content above the telescope. Cloud cover constitutes the most obvious example, but more subtle changes in the column density of scatterers can generate large effects. Figure 8

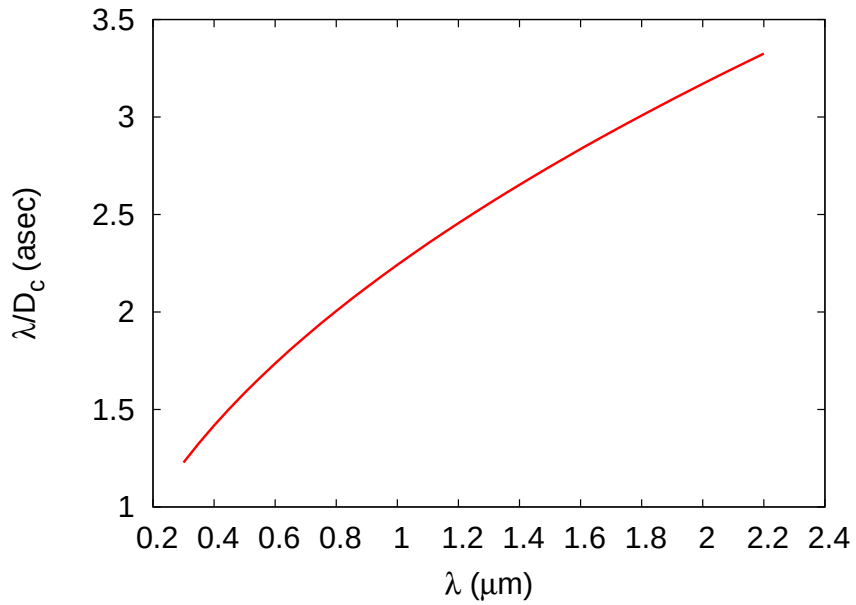

Figure 7: Plot of the critical radius corresponding to the lateral coherence scale as a function of observing wavelength. This is the characteristic radius to which light is scattered by the effects of scintillation.

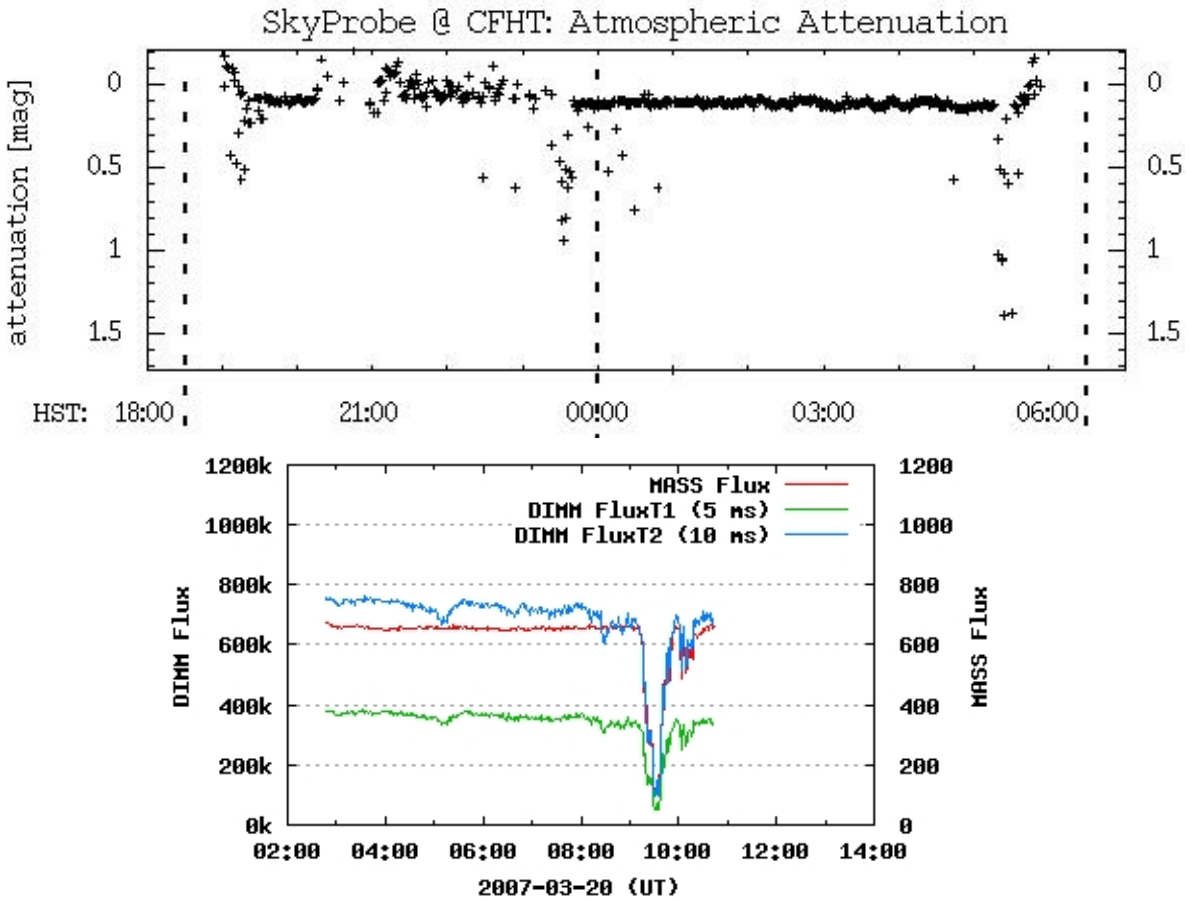

Figure 8: Illustrations of variable atmospheric attenuation observed in the visible. The left frame shows data taken with SkyProbe on the Canada France Hawaii Telescope (http://www.cfht.hawaii.edu/Instruments/Elixir/skyprobe/about.html). This instrument measures the flux of several hundred stars in the telescope pointing direction once a minute to derive a measure of atmospheric attenuation. On the left is shown raw counts recorded by the DIMM/MASS turbulence monitoring system at Palomar Observatory (http://odata1.palomar.caltech.edu/massdimm/). This system tracks Polaris throughout the night, and displays variability in atmospheric attenuation. Temporal variability in atmospheric attenuation like that illustrated in these data can induce large systematic errors, particularly in applications requiring absolute photometry.

displays measurements of the atmospheric attenuation taken at ≈ 1 minute intervals over a single night. This variability can clearly induce substantial, systematic variations in measurements of the absolute photometry. Measurements of the differential photometry of objects within a single frame should be much less sensitive to variable atmospheric attenuation.

4.3 Field Dependent Aberrations

Field dependent aberrations arising within the adaptive optics system or downstream instrumentation generate field dependent evolution of the PSF. Common observing strategies such as rotation of the field or dithering the field on the chip may induce variations in the PSFs of targets in the field of view. Depending on the character of the observation, these distortions may induce systematic errors in the measured photometry that are difficult to quantify, at least in the absence of a specific optical design. These aberrations may evolve as the telescope and instrumentation is subjected to a changing gravity load.

Another source of aberration particular to adaptive optics systems arises from non-common path errors between the science camera and the wavefront sensor. In an AO system, light is separated and directed into these optical paths by a dichroic. The adaptive optics system drives the deformable mirror so as to minimize phase errors seen by the wavefront sensor, including any static optical aberrations that arise in the wavefront sensor optics. These aberrations are not present in the science path, and so the AO system can act to distort the wavefront seen by the science camera. Such non-common path errors can generate field and time dependent PSF evolution across the science camera that may induce systematic errors in photometric applications.

4.4 Detector Effects

There is a large body of literature on CCD[23] and infrared[24] detectors and their use in astronomy. Of the many features displayed by these devices, there is a substantial list of effects that can impact photometric accuracy. These include read noise, dark current, bad pixels, variability in pixel responsivity, cosmic rays, and responsivity that depends on incident flux. The discretization that occurs when imaging an object with a discrete array of pixels also introduces sampling considerations in deconvolution algorithms. As an illustrative example, an analysis that aims to account for discrete sampling that arises from detector arrays has been developed by Mighell[25].

Of the wealth of experimental results that have been published using astronomical detectors, the diffraction limited regime in which the Hubble Space Telescope operates is in many ways most closely analogous to ground based adaptive optics. It is worth

noting that WFPC2 has demonstrated photometric stability on calibration stars of 1.5% over seven years of operation. Considering the large number of effects specific to ground based observations that have been described above, it seems unlikely that additional efforts above and beyond securing modern CCD and IR detectors for NGAO could be justified on the basis of hypothetical improvements to photometric accuracy. Any effort to place additional requirements on these detectors could entail significant budgetary consequences.

5 Case Study-Stellar Populations in Nearby Galaxies

In the previous section, a number of effects that degrade photometric accuracy were described. To illustrate the manner in which these considerations enter in a particular application, this section presents a case study of photometric measurements of stellar populations in nearby galaxies.

5.1 Background

The major focus of modern stellar populations research is the understanding of the formation and evolution of galaxies within the context of the large-scale structure of the expanding universe. One way to approach the problem is to observe ensembles of galaxies forming and evolving as a function of redshift, or lookback time; another is to study the star-forming histories of entire galaxies from their resolved individual stars. Both methods have complementary strengths. The high redshift approach has inherently higher time resolution at early times, but is limited by the faintness of distant objects and provides only a snapshot taken at a single time of individual galaxies. The individual star approach yields the complete star formation histories of galaxies, but is limited by the ability of telescopes to resolve dense star fields. Current observations are such that the two approaches do not quite overlap. The known galaxies at high redshift are destined to become the high surface brightness components of massive galaxies, which have been difficult to impossible to resolve locally, whereas the nearby galaxies and galactic components for which we have complete star formation histories are too low in surface brightness to appear in high redshift surveys. Increasing the resolving power and ability to measure precise photometry in crowded star fields with the largest available telescopes, as envisioned by Keck NGAO, will go a long way towards joining the two approaches and providing a more robust and complete description of galaxy formation and evolution.

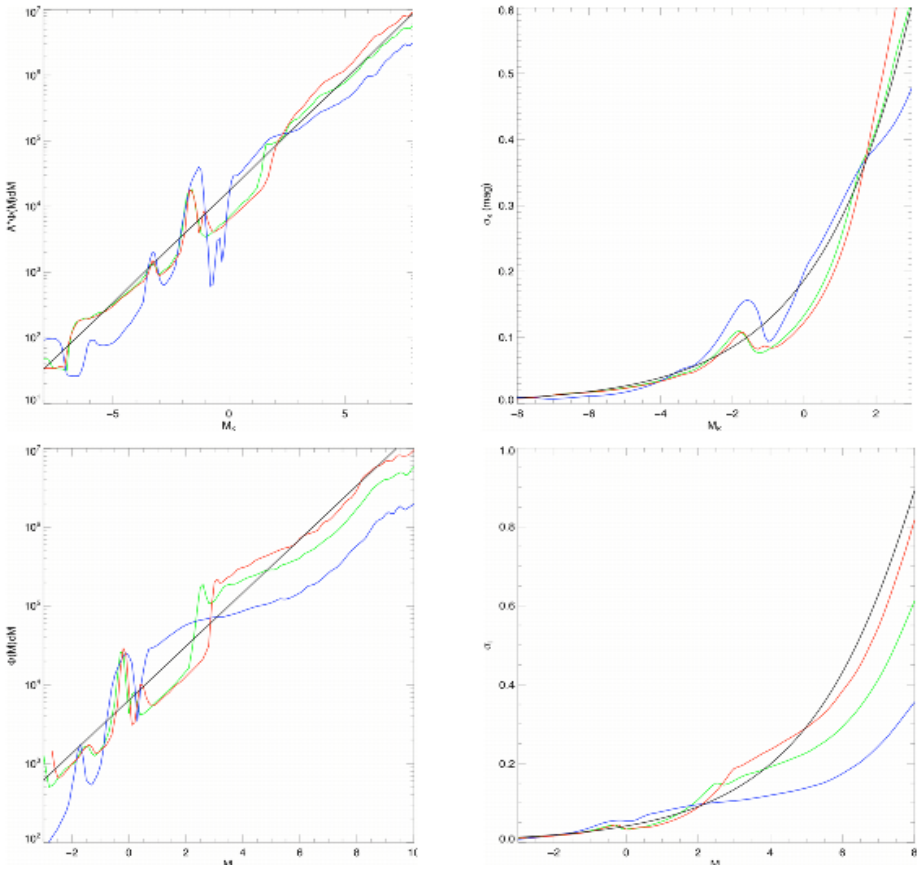

Figure 9: Top left: Power-law luminosity function $\Phi(L) \propto L^{-1.85}$ (black line) compared to K-band luminosity functions drawn from Padova isochrones with ages 1 Gyr (blue), 5 Gyr (green), and 10 Gyr (red) and solar metallicity. The normalization has been set to show the number of stars per magnitude found in a field with size 30"x30", surface brightness $\Sigma_K = 18$ mags arcsec^{-2}, and distance modulus $(m - M)_0$=24.45. Top right: Photometric error due to crowding for the LFs shown at top left, assuming a resolution element of λ/D. In practice, photometry with crowding-induced error of <0.1 mag is generally ∼100% complete, with completeness falling to 50% at σ ∼0.2 mag. Bottom: As above, but for I-band.

5.2 Modeling the Error due to Crowding

From Olsen, Blum, & Rigaut[27], the following expression relates the surface brightness of the environment, the distance modulus, the photometric error, and the stellar magnitude

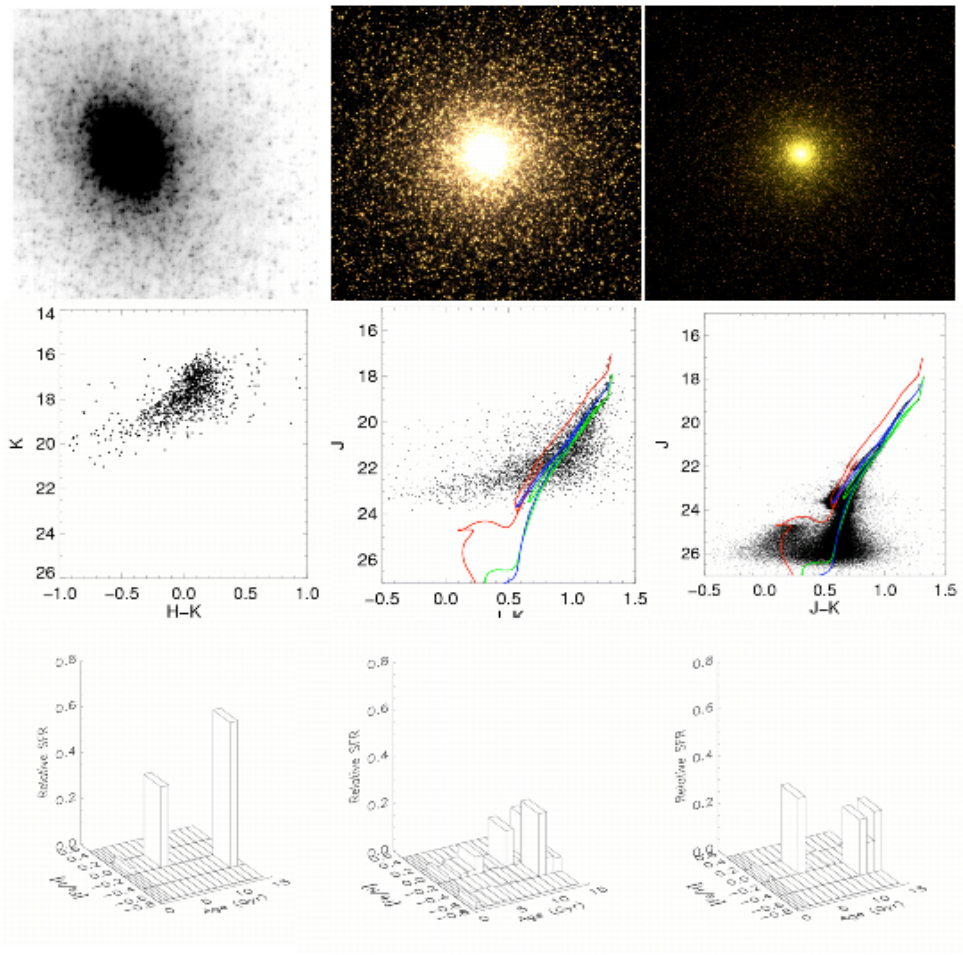

Figure 10: Stellar populations at the center of M32. Top row, left to right: images of the central 30" of M32 as observed with Gemini N+Hokupa'a (Davidge et al.[26]) and as simulated with JWST and a 30-m GSMT. Middle row, left to right: Color-magnitude diagrams of M32 corresponding to the images in the top row. Bottom row: The population box used to create the JWST and GSMT simulations is shown at left, while the recovered JWST and GSMT population mixes are shown in the middle and right panels.

for a general luminosity function $\Phi(M)$, under the assumption that all of the photometric error is due to crowding:

$$\Sigma_m > 2M - 2.5 \log \left[\frac{4}{\pi} \left(\frac{\sigma_m}{1.086 a_{\rm res}} \right)^2 \times \frac{\int_{M_{lo}}^{M_{hi}} 10^{-0.4M\prime} \Phi\left(M\prime\right) dM\prime}{\int_{M_{lo}}^{M} 10^{-0.8M\prime} \Phi\left(M\prime\right) dM\prime} \right] + (m-M)_0 \qquad (9)$$

If we adopt a luminosity function $\Phi(L) \propto L^{\alpha}$ (such that $\log_{10} \Phi(M) = -0.4(\alpha+1)M +$ const.), then we get a clean analytical expression for the crowding-induced photometric error σ_m:

$$\sigma_m = 10^{-0.2(\Sigma_m - (m-M)_0 - 2M + M_{lo})} \left(\frac{1.086 a_{\rm res}}{2} \sqrt{\pi \frac{(2+\alpha)(10^{-0.4(3+\alpha)(M-M_{lo})} - 1)}{(3+\alpha)(10^{-0.4(2+\alpha)(M_{hi}-M_{lo})} - 1)}} \right) \qquad (10)$$

For stellar populations with ages $>\sim$3 Gyr in the near-infrared, $\alpha = -1.85$ is a good approximation to a luminosity function drawn from a Salpeter IMF. In Figure 9, the power-law luminosity function $\Phi(L) \propto L^{-1.85}$ (black line) is compared to K- and I-band luminosity functions with ages 1 Gyr (blue line), 5 Gyr (green line), and 10 Gyr (red line) and solar metallicity, as calculated from Padova isochrones. Figure 10 shows an example of the corresponding crowding-induced photometric errors vs. K and I magnitude, assuming $\Sigma_K = 18$ mags arcsec^{-2} (appropriate for the disk of M31 $\sim 10\prime$ from the center), I-K=1.9, $(m-M)_0$=24.45, and a diffraction-limited 10-m telescope. For the discrete ages, the calculation was done numerically using Equation 9, while for the power-law LF, the purely analytical Equation 10 was used. The example demonstrates that in the disk of M31, Keck NGAO should be capable of providing useful photometry ($\sigma \sim$0.1) at the level of the horizontal branch (K$\sim$23) in K, and at the level of the subgiant branch of a 5 Gyr-old population in I (I$\sim$27). Reaching these depths will take only a few to a few tens of minutes of exposure time in this particular example, but will allow the measurement of the star formation history of M31's high surface brightness disk and bulge with unprecedented detail, as described next.

5.3 The Effect of Depth on Recovered Star Formation Histories

To demonstrate the effect of increased resolution on photometric depth in crowded fields and the dramatic increase in ability to disentangle the mix of stellar populations that galaxies contain, I will simply refer to the work done by us as part of studies for the GSMT Science Working Group. Figure 10 includes an observation of the center of the nearby dwarf elliptical galaxy M32 obtained with the Gemini North telescope and Hokupa'a/QUIRC AO-corrected near-infrared camera (Davidge et al.[26]) as well as simulations of the performance of JWST and a 30-m GSMT for the same observation. The

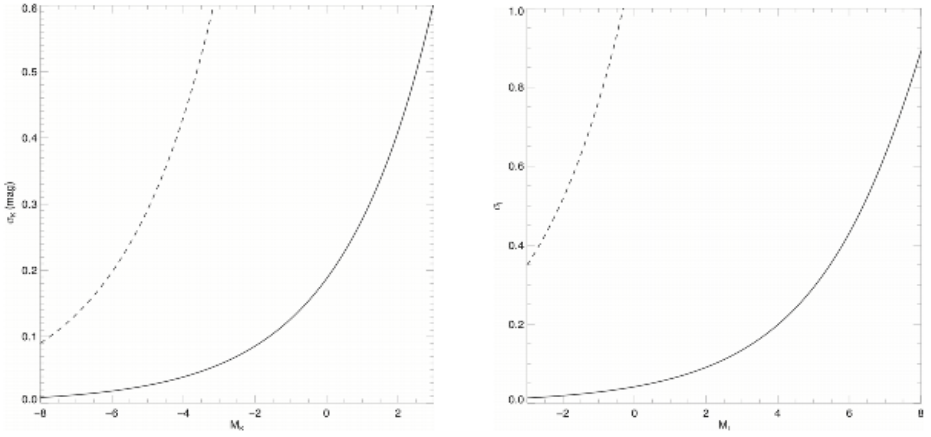

Figure 11: Left: Photometric error in K due to crowding for the power law LF $\Phi(L) \propto L^{-1.85}$ shown in Figure 9, assuming a resolution element of l/D (solid line) and 1 arcsec (dashed line). For the 1 arcsec-scale curve, the error has been reduced by 50% compared to the result of equation 2 in order to account for the subtraction of the PSF cores of faint stars within the 1 arcsec aperture. Right: As on the left, but for I-band and for a 0.5 arcsec aperture (dashed line) rather than the 1 arcsec aperture used on the left.

JWST color-magnitude diagram goes almost no deeper than the Hokupa'a observation, revealing only the brightest evolved stars, while the GSMT observation approaches the old main sequence turnoff. The gain in the recovered star formation history provided by the GSMT in this case is clear; whereas JWST provides the correct qualitative features, GSMT measures the star formation history with high precision.

These results are directly applicable to the example Keck NGAO observation used in the previous section. A 30-m GSMT will reach a depth of J$\sim$26 at the center of M32. In the disk of M31, Keck NGAO will reach a similar depth in J and still deeper in I, and thus should be able to measure M31's disk star formation history in excellent detail. The addition of I-band in the Keck NGAO system will also provide a gain in ability to discriminate stellar populations through increased temperature sensitivity, a point that remains to be addressed through simulations specifically targeted for Keck NGAO.

5.4 Calibration considerations

As described elsewhere in this document, the spatial and temporal variability of AO-corrected PSFs makes calibration a particularly important issue for photometry. Uncor-

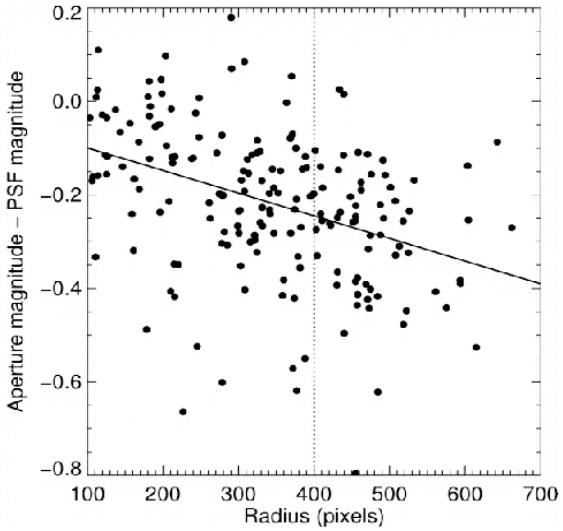

Figure 12: Aperture corrections as a function of radius for the M31 bulge images studied by Olsen et al.[27]. The differences between the magnitudes measured within a 0.7" diameter aperture and the PSF-fit magnitudes are plotted vs. radius from the central guide star. Anisoplanicity produces a strong radial dependence of the aperture correction. Figure reproduced from Olsen et al.[27].

rected anisoplanatism introduces scatter in measured color-magnitude diagrams, while uncertainty in the time variability of the PSF translates to zero point uncertainty. In the case of crowded field observations of nearby galaxies, however, we should be able to correct for much of the PSF variability using simple photometric measurements on the images themselves. The technique is straightforward and standard in crowded field photometry. PSF-fitting photometry is first performed on the narrow cores of all stars in the field. These fits are then used to subtract the cores of all stars from the image with the exception of the few hundred brightest unsaturated stars, which are left untouched. Aperture photometry with diameter $\sim$1 arcsec is then measured for these brightest stars, and used to construct an aperture correction for the PSF photometry as a function of radius from the AO guide star. Standard star photometry out to the same diameter is then used to convert the aperture-corrected PSF photometry to standard magnitudes. While a 1-arcsec aperture will not capture all of the light in the PSF, it will contain the majority of the PSF variability. Aperture photometry on the standard stars out to much larger diameters can be used to investigate the level at which the PSF wings outside $\sim$1

arcsec are variable, which for Gemini North and NIRI+Altair was found to be ∼0.05-0.1 mag (Olsen et al.[27]), reflecting the uncertainty in the zero point of the photometry. Interleaving science and standard star observations could reduce this residual zero point uncertainty further.

Why should this procedure work? The dominant source of error for the 1 arcsec diameter point source photometry of bright stars is clearly crowding, which produces fluctuations in the stellar background at the scale of ∼1 arcsec. Subtracting the PSF cores of all stars other than the bright stars under consideration reduces the scale of these fluctuations, but does not eliminate them on account of the significant contribution of the broad PSF wings. We thus need to compute the photometric error due to crowding for the brightest few hundred stars at the scale of ∼1 arcsec, with the crowding error reduced by roughly the fraction of encircled energy in the PSF core compared to the total to account for the subtraction of the cores of fainter stars. Following the M31 example used in section 2 above, Figure 11 shows the crowding error at the scale of the diffraction limit for K and I and at the 1 arcsec scale (K) and 0.5 arcsec scale (I), assuming that PSF core subtraction reduces the crowding error at the 1 arcsec scale by 50% in K, and at the 0.5 arcsec scale by 10% in I. From Figure 9, we see that there are a few hundred stars with magnitude $M_K \leq$-6 and with $M_I \leq$-2.5. From Figure 11, the crowding-induced photometric errors for these stars is $\sigma_K \leq$0.2 and $\sigma_I \leq$0.4 individually. While these errors are large on a per-star basis, by averaging the results from several hundred stars, the uncertainty in the correction for the spatial variability of the PSF will be roughly an order of magnitude lower. The larger error in the I-band aperture photometry despite the smaller aperture suggests that Keck NGAO I-band observations may need to be restricted to the best seeing conditions in order for the above procedure to work.

For a demonstration of this technique, Figure 12 shows the aperure correction as a function of radius measured by us from K-band Gemini North NIRI+Altair images of the bulge of M31 (Olsen et al.[27]), where we used the technique for deriving the aperture correction as described above. The scatter in the individual photometry of bright stars is large (∼0.15 mag), as we would expect from the crowding in the image, but the uncertainty in the aperture correction is only ∼0.03 mag.

6 PSF Estimation Algorithms

At least in principle, knowledge of the PSF delivered by an adaptive optics system would permit deconvolution of the observed data. Such an approach would permit direct extraction of photometry from observations of point sources and extended objects. Deconvolution is clearly preferable to aperture photometry in a wide variety of applications,

including photometry of crowded stellar fields and resolved targets. To pursue a deconvolution approach typically requires a measurement or an estimate of the PSF. Recent results in the area of AO PSF estimation are reviewed in this section. Efforts to apply deconvolution algorithms to astronomical data, including blind and myopic deconvolution techniques, are discussed in the following section.

6.1 Estimation of the Guide Star PSF

Knowledge of the guide star PSF for a single conjugate adaptive optics system permits deconvolution of the observation for objects that lie within the isoplanatic patch. Algorithms that provide an estimate of the guide star PSF have been developed in a number of studies[28, 29, 30]. These algorithms aim to estimate the long exposure optical transfer function (OTF) delivered by the adaptive optics system. This OTF suffers from the inability of the adaptive optics system to perfectly compensate wavefront errors within its spatial control bandwidth, and its inability to compensate errors that arise outside of its spatial control bandwidth. The former errors may be estimated from telemetry data, while the latter may be computed under the assumption of Komolgorov turbulence. Using this estimation of the guide star OTF, the PSF may be computed by Fourier transformation. This approach has been tested experimentally on adaptive optics systems using both curvature [28] and Shack Hartmann[31] wavefront sensors. Guide star PSF predictions for AO systems using the former type of sensor have been pursued for a longer period of time, and have generally been in better agreement with experiment.

6.2 Field Dependent PSF Estimation

For observations of fields larger than the isoplanatic patch, the AO PSF displays field dependent evolution arising from anisoplanatism. In this regime, estimates of the guide star PSF cannot be used for deconvolving science targets outside the isoplanatic patch, and alternative approaches must be used to predict the field dependent PSF of the AO system. A number of different techniques have been used to generate such predictions.

Semiempirical approaches to generating PSF predictions for NGS[32] and LGS[33] observations have been developed. In these approaches, observations of dense star fields are interspersed with those of the science target cfields. The former observations are used to form a map of the field dependent PSF delivered by the adaptive optics system, which may be used to deconvolve the science data. PSF predictions formed using this procedure have demonstrated agreement with NGS AO observations at the Canada France Hawaii Telescope and on the 3m Shane Telescope at Lick Observatory to the level of 20% in

the FWHM of the PSF[32], and agreement with LGS AO observations on the 3m Shane Telescope to the level of 10% in Strehl ratio[33].

Approaches to modeling the field dependent AO PSF have been pursued in other studies. Cresci *et al.* [18] used observations of a crowded stellar field to determine the parameters of a constrained model that accounted for anisoplanatism. The assumption in this model was that the anisoplanatic kernel was an elliptical gaussian, and the radial and tangential widths of this gaussian as a function of angular offset from the guide star were derived from the calibration fields. These results were used to model the field dependent PSF in image data obtained at the VLT using NAOS/CONICA. Aubailly [34] used a similar technique in analyzing the effects of anisoplanatism on binary observations acquired with the 3.6m Advanced Electro Optical System Telescope.

Sheehy *et al.* [35] performed photometry on crowded stellar fields observed using the laser guide star AO system at Keck Observatory. In this research, the measured modulation transfer function of the observation was used together with a model of the OTF delivered by the adaptive optics system to derive photometry of cluster members. Photometric measurements were shown to be consistent with data from the Hubble telescope to an accuracy of a few percent.

The model in Equation 1 has been applied in measuring the differential photometry of binary and multiple star systems[12, 36]. In these studies, $OTF_{gs}(\vec{r})$ was measured from the observations by extracting and Fourier transforming the guide star point spread function. The anisoplanatic structure function was computed from Equation 2 using a measured turbulence profile and the values for k, $\vec{\theta}$, aperture diameter, and zenith angle appropriate for the observation. In this approach there are no free parameters in the predicted PSF. Using near-IR observations of a 21 asec binary, model predictions of the binary companion Strehl ratio have been demonstrated to agree with measured values to accuracies of order 1%, as these Strehl ratios evolved between 5% and 30% in response to temporal evolution in the atmospheric turbulence and wind profiles[12]. This study also demonstrated measurements of the differential photometry of the binary system stable to 1% in a 1.4 sec integration, with an estimated error in the mean of .1% over the course of the three hour experiment.

The use of the measured guide star PSF and an anisoplanatic structure function to capture the complex evolution of the AO PSF in time, field location, and wavelength consitutes a powerful technique for the reduction of natural guide star adaptive optics observations. This technique allows one to extend the field of view over which the PSF may be estimated beyond the isoplanatic patch. This permits application of the model over the arcminute fields of view that are typically imaged by the current generation of adaptive optics systems and near-IR cameras. The use of this self-referencing algorithm permits one to formulate PSF predictions from a single observation, without the need for a

separate observation of a PSF reference star. This is important not only for observational efficiency, but also due to the fact that the turbulence profile may evolve between science and calibration observations. As indicated by the Strehl ratio evolution in Figure 3, this evolution can seriously impact the utility of the calibration PSF. Finally, there are no free parameters in the PSF prediction, which facilitates automation of the algorithm.

6.3 PSF Monitoring Camera

A number of techniques described above benefit from contemporaneous images of a reference PSF. This can be a significant restriction in the application of these techniques to observations. Ideally, the reference PSF and science target should be close enough on the sky to permit simultaneous imaging. This avoids the observational overhead of imaging a separate guide star, and avoids errors arising from evolution of the system performance between observations. Existing adaptive optics systems typically offer multiple plate scales, and for deconvolution algorithms it is desirable to Nyquist sample or oversample the image. This sampling restriction tends to drive observations towards smaller fields of view, which places strong restrictions on observable targets. A second difficulty arises from the fact that PSF calibration cannot be performed using saturated data. This places a restriction on the differential magnitude between the guide star and the science target. Hawaii 2 RG chips permit rapid readout of small regions of interest within the detector, and in principle this capability may be used to rapidly read out the section of the chip containing the guide star PSF, thereby avoiding saturation. From a practical perspective this would entail additional development effort to support this mode of operation in existing and/or future astronomical instrumentation.

The use of a PSF monitoring camera that could be deployed independently of the science camera affords a solution to both of the above problems. By deploying this camera to image the guide star while the primary camera is used for the science target, restrictions on field of view and plate scale may be avoided. The use of two separate cameras permits independent exposure times for the guide star and science targets, alleviating restrictions on the differential magnitude of the two objects.

7 Deconvolution Algorithms

Deconvolution is a broad, multidisciplinary subject. This section lists deconvolution algorithms that have been developed and used in adaptive optics imaging applications. The section also summarizes literature in which the performance of algorithms were compared directly on astronomical adaptive optics data.

Blind and myopic deconvolution algorithms aim to extract estimates of the PSF from the data, while at the same time generating estimates of the source flux distribution. The term myopic represents the notion that the PSF is unknown, but certain constraints such as positivity and band limitations arising from the finite telescope aperture may be enforced in a solution. A number of algorithms for performing blind [37] and myopic [38, 39, 40, 41] deconvolution exist in the literature, and have been applied to Keck observations of Io [1, 42].

Parametric blind deconvolution algorithms enforce a model for the PSF as part of the deconvolution procedure. Algorithms have been developed that model the PSF as a Lorentzian [43] or a Lorentzian plus an Airy function [44].

Specialized algorithms have been developed for the deconvolution of crowded stellar fields. Starfinder[45] is a code that performs deconvolution of crowded stellar fields. This code assumes a constant PSF over the field and extracts photometry and astrometry for stars within an isoplanatic patch.

Deconvolution of crowded stellar fields larger than the isoplanatic patch has been performed by Britton[36]. In this analysis, measurements of the turbulence profile were used to estimate the degradation of the field dependent point spread function arising from anisoplanatism. By using the guide star as a PSF reference and incorporating a measurement of the turbulence profile in accounting for anisoplanatism, a prediction of the field dependent PSF could be generated over fields much larger than the isoplanatic patch. These predictions were used in the deconvolution of a crowded stellar field at angular offset of 12 asec from the guide star.

A few studies have aimed to compare methods for deconvolution. Christou *et al.*[14] have compared the performance of blind deconvolution, Starfinder, and parametric blind deconvolution in observations of the Galactic Center acquired with the Hokupaa AO system on the Gemini telescope. This comparison indicated that these techniques were consistent down to 4 stellar magnitudes of dynamic range, but began to diverge for stars fainter than this limit. de Pater *et al.*[1] have compared Starfinder with blind and myopic deconvolution codes in observations of volcanoes on Io. These results indicate a level of consistency among these codes of order .1 mag in K band, with much worse agreement in L band.

8 Summary

The use of adaptive optics in applications that require quantitative photometric measurements is a relatively young field in ground based astronomy. The observational targets themselves are broadly distributed, from planetary to extragalactic sources and from point

sources to extended emission regions. For many of these applications, deconvolution constitutes the key analytical technique for establishing the distribution of flux in the focal plane. Critical to the application of this technique is a knowledge of the PSF delivered by the adaptive optics system. Variations in the PSF delivered by an adaptive optics system occur in time, field location and wavelength, and are much more pronounced than in seeing limited instruments. This PSF variability is inextricably linked to variability of the turbulence and wind profiles above the telescope, which themselves vary in an uncontrolled manner. Because of this, requirements for photometric precision and accuracy that may be placed on an adaptive optics system by its users are difficult to translate into instrumental requirements. Current research in this field is aimed towards establishing characteristic levels of photometric stability that may be achieved using adaptive optics systems on ground based telescopes. While this situation may appear discouraging, published results suggest that with effort, differential photometry at the level of .1% to 1% may be achieved on ground based telescopes - at least for binary star observations. This level of performance is astronomically attractive, and NGAO should look towards establishing an instrument design that does not preclude this level of photometric accuracy. The four recommendations below constitute suggestions as to how Keck Observatory can help to ensure the best photometric outcome for NGAO.

9 Recommendations and Future Work

- Require turbulence monitoring capabilities that deliver C_n^2 measurement on minute timescales. Measurements from a turbulence monitor will establising a baseline of C_n^2 profiles that may be used to understand both mean turbulence conditions and the degree of variability about the mean. This will help to establish expectations for photometric stability. An understanding of the turbulence conditions under which NGAO is operating will significantly aid both operators and observers in making decisions on target selection and observing strategy. Use of turbulence profiles in postprocessing algorithms also shows promise in improving photometric precision.

- Consider providing an auxiliary camera for contemporaneous measurements of the PSF. The purpose of this camera would be to perform observations of a reference point source for use in deconvolution of data from the science camera. The exact requirements on this camera would depend upon the adaptive optics architecture selected for NGAO and the photometric requirements ultimately placed on the system. But to be useful this camera should be Nyquist sampled and should be deployable independently of the science detector. This camera should also be deployable over

a field large enough to find a point source reference for PSF calibration.

- As a step towards understanding the requirements for this auxiliary PSF camera, consider conducting NIRC2 and/or OSIRIS imaging camera experiments with the existing single conjugate AO system and the T6 DIMM/MASS turbulence profile equipment. These experiments will indicate the utility of contemporaneous PSF measurements, and may provide near term benefits for Keck Observatory.

- Consider providing facility deconvolution pipelines for Keck NGAO data. This is a more efficient alternative than having each observing team reimplement these techniques as part of their research effort, and could improve the quality and quantity of scientific output from Keck Observatory.

References

[1] I. de Pater, F. Marchis, B. A. Macintosh, H. G. Roe, D. Le Mignant, J. R. Graham, and A. G. Davies, "Keck AO observations of Io in and out of eclipse," *Icarus* **169**, pp. 250–263, May 2004.

[2] S. G. Gibbard, I. de Pater, and H. B. Hammel, "Near-infrared adaptive optics imaging of the satellites and individual rings of Uranus," *Icarus* **174**, pp. 253–262, Mar. 2005.

[3] I. de Pater, M. Ádámkovics, A. H. Bouchez, M. E. Brown, S. G. Gibbard, F. Marchis, H. G. Roe, E. L. Schaller, and E. Young, "Titan imagery with Keck adaptive optics during and after probe entry," *Journal of Geophysical Research (Planets)* **111**, pp. 7– +, June 2006.

[4] N. E. B. Zellner, S. Gibbard, I. de Pater, F. Marchis, and M. J. Gaffey, "Near-IR imaging of Asteroid 4 Vesta," *Icarus* **177**, pp. 190–195, Sept. 2005.

[5] F. Marchis, M. Kaasalainen, E. F. Y. Hom, J. Berthier, J. Enriquez, D. Hestroffer, D. Le Mignant, and I. de Pater, "Shape, size and multiplicity of main-belt asteroids," *Icarus* **185**, pp. 39–63, Nov. 2006.

[6] S. Gillessen, F. Eisenhauer, E. Quataert, R. Genzel, T. Paumard, S. Trippe, T. Ott, R. Abuter, A. Eckart, P. O. Lagage, M. D. Lehnert, L. J. Tacconi, and F. Martins, "Variations in the spectral slope of Sgr A* during a NIR flare," *Journal of Physics Conference Series* **54**, pp. 411–419, Dec. 2006.

[7] J. D. Hartman, K. Z. Stanek, B. S. Gaudi, M. J. Holman, and B. A. McLeod, "Pushing the Limits of Ground-based Photometric Precision: Submillimagnitude Time-Series Photometry of the Open Cluster NGC 6791," *AJ* **130**, pp. 2241–2251, Nov. 2005.

[8] I. A. G. Snellen, "High-precision K-band photometry of the secondary eclipse of HD 209458," *MNRAS* **363**, pp. 211–215, Oct. 2005.

[9] F. Pont, C. Moutou, M. Gillon, A. Udalski, F. Bouchy, J. Fernandes, W. Gieren, M. Mayor, T. Mazeh, D. Minniti, C. Melo, D. Naef, G. Pietrzynski, D. Queloz, M. T. Ruiz, N. Santos, and S. Udry, "ESO Large Programme 666 on OGLE transits: I. Accurate radius of the planets OGLE-TR-10b and OGLE-TR-56b with VLT deconvolution photometry," *ArXiv Astrophysics e-prints* , Oct. 2006.

[10] J.-P. Beaulieu, D. P. Bennett, P. Fouqué, A. Williams, M. Dominik, U. G. Jorgensen, D. Kubas, A. Cassan, C. Coutures, J. Greenhill, K. Hill, J. Menzies, P. D. Sackett, M. Albrow, S. Brillant, J. A. R. Caldwell, J. J. Calitz, K. H. Cook, E. Corrales, M. Desort, S. Dieters, D. Dominis, J. Donatowicz, M. Hoffman, S. Kane, J.-B. Marquette, R. Martin, P. Meintjes, K. Pollard, K. Sahu, C. Vinter, J. Wambsganss, K. Woller, K. Horne, I. Steele, D. M. Bramich, M. Burgdorf, C. Snodgrass, M. Bode, A. Udalski, M. K. Szymański, M. Kubiak, T. Więckowski, G. Pietrzyński, I. Soszyński, O. Szewczyk, Ł. Wyrzykowski, B. Paczyński, F. Abe, I. A. Bond, T. R. Britton, A. C. Gilmore, J. B. Hearnshaw, Y. Itow, K. Kamiya, P. M. Kilmartin, A. V. Korpela, K. Masuda, Y. Matsubara, M. Motomura, Y. Muraki, S. Nakamura, C. Okada, K. Ohnishi, N. J. Rattenbury, T. Sako, S. Sato, M. Sasaki, T. Sekiguchi, D. J. Sullivan, P. J. Tristram, P. C. M. Yock, and T. Yoshioka, "Discovery of a cool planet of 5.5 Earth masses through gravitational microlensing," *Nature* **439**, pp. 437–440, Jan. 2006.

[11] L. C. Roberts, Jr., N. H. Turner, L. W. Bradford, T. A. ten Brummelaar, B. R. Oppenheimer, J. R. Kuhn, K. Whitman, M. D. Perrin, and J. R. Graham, "Adaptive Optics Photometry and Astrometry of Binary Stars," *AJ* **130**, pp. 2262–2271, Nov. 2005.

[12] M. C. Britton, "The Anisoplanatic Point-Spread Function in Adaptive Optics," *PASP* **118**, pp. 885–900, June 2006.

[13] J. C. Christou and J. D. Drummond, "Measurements of Binary Stars, Including Two New Discoveries, with the Lick Observatory Adaptive Optics System," *AJ* **131**, pp. 3100–3108, June 2006.

[14] J. C. Christou, G. Pugliese, R. Köhler, and J. D. Drummond, "Photometric and Astrometric Analysis of Gemini/Hokupa'a Galactic Center Adaptive Optics Observations," *PASP* **116**, pp. 734–744, Aug. 2004.

[15] R. S. Ellis, "Observations of the high redshift universe," 2007.

[16] J. Melbourne, S. A. Wright, M. Barczys, A. H. Bouchez, J. Chin, M. A. van Dam, S. Hartman, E. Johansson, D. C. Koo, R. Lafon, J. Larkin, D. Le Mignant, J. Lotz, C. E. Max, D. M. Pennington, P. J. Stomski, D. Summers, and P. L. Wizinowich, "Merging Galaxies in GOODS-S: First Extragalactic Results from Keck Laser Adaptive Optics," *ApJL* **625**, pp. L27–L30, May 2005.

[17] D. C. Koo, J. Melbourne, C. Max, A. Metevier, M. Ammons, J. E. Larkin, M. Barczys, S. A. Wright, and E. Steinbring, "CATS: CfAO Treasury Survey of distant galaxies, supernovae, and AGN's," *ArXiv Astrophysics e-prints* , Mar. 2007.

[18] G. Cresci, R. I. Davies, A. J. Baker, and M. D. Lehnert, "Accounting for the anisoplanatic point spread function in deep wide-field adaptive optics images," *A&A* **438**, pp. 757–767, Aug. 2005.

[19] G. Cresci, R. I. Davies, A. J. Baker, F. Mannucci, M. D. Lehnert, T. Totani, and Y. Minowa, "Galaxy morphology and evolution from SWAN adaptive optics imaging," *A&A* **458**, pp. 385–396, Nov. 2006.

[20] S. A. Wright, J. E. Larkin, M. Barczys, D. K. Erb, C. Iserlohe, A. Krabbe, D. R. Law, M. W. McElwain, A. Quirrenbach, C. C. Steidel, and J. Weiss, "Integral Field Spectroscopy of a Candidate Disk Galaxy at z ˜ 1.5 Using Laser Guide Star Adaptive Optics," *ApJ* **658**, pp. 78–84, Mar. 2007.

[21] T. Fusco, J.-M. Conan, L. M. Mugnier, V. Michau, and G. Rousset, "Characterization of adaptive optics point spread function for anisoplanatic imaging. Application to stellar field deconvolution," *Astronomy and Astrophysics Supplement* **142**, pp. 149–156, Feb. 2000.

[22] S. L. Kenyon, J. S. Lawrence, M. C. B. Ashley, J. W. V. Storey, A. Tokovinin, and E. Fossat, "Atmospheric Scintillation at Dome C, Antarctica: Implications for Photometryand Astrometry," *PASP* **118**, pp. 924–932, June 2006.

[23] J. R. Janesick, *Scientific charge-coupled devices*, Scientific charge-coupled devices, Bellingham, WA: SPIE Optical Engineering Press, 2001, xvi, 906 p. SPIE Press monograph, PM 83. ISBN 0819436984, 2001.

[24] J. D. Vincent, ed., *Fundamentals of infrared detector operation and testing*, New York : Wiley, 2001.

[25] K. J. Mighell, "Stellar photometry and astrometry with discrete point spread functions," *MNRAS* **361**, pp. 861–878, Aug. 2005.

[26] T. J. Davidge, F. Rigaut, M. Chun, W. Brandner, D. Potter, M. Northcott, and J. E. Graves, "The Peak Brightness and Spatial Distribution of Asymptotic Giant Branch Stars Near the Nucleus of M32," *ApJL* **545**, pp. L89–L92, Dec. 2000.

[27] K. A. G. Olsen, R. D. Blum, and F. Rigaut, "Stellar Crowding and the Science Case for Extremely Large Telescopes," *AJ* **126**, pp. 452–471, July 2003.

[28] J. P. Veran, F. Rigaut, H. Matre, and D. Rouan, "Estimation of the adaptive optics long-exposure point-spread function using control loop data," *JOSA A* **14**, p. 3057, 1997.

[29] J. Marino, T. R. Rimmele, and J. C. Christou, "Long-exposure point spread function estimation from adaptive optics loop data," in *Advancements in Adaptive Optics. Edited by Domenico B. Calia, Brent L. Ellerbroek, and Roberto Ragazzoni. Proceedings of the SPIE, Volume 5490, pp. 184-194 (2004).*, D. Bonaccini Calia, B. L. Ellerbroek, and R. Ragazzoni, eds., pp. 184–194, Oct. 2004.

[30] E. Gendron, Y. Clénet, T. Fusco, and G. Rousset, "New algorithms for adaptive optics point-spread function reconstruction," *A&A* **457**, pp. 359–363, Oct. 2006.

[31] L. Jolissaint, J.-P. Veran, and J. Marino, "OPERA, an automatic PSF reconstruction software for Shack-Hartmann AO systems: application to Altair," in *Advancements in Adaptive Optics. Edited by Domenico B. Calia, Brent L. Ellerbroek, and Roberto Ragazzoni. Proceedings of the SPIE, Volume 5490, pp. 151-163 (2004).*, D. Bonaccini Calia, B. L. Ellerbroek, and R. Ragazzoni, eds., pp. 151–163, Oct. 2004.

[32] E. Steinbring, S. M. Faber, S. Hinkley, B. A. Macintosh, D. Gavel, E. L. Gates, J. C. Christou, M. Le Louarn, L. M. Raschke, S. A. Severson, F. Rigaut, D. Crampton, J. P. Lloyd, and J. R. Graham, "Characterizing the Adaptive Optics Off-Axis Point-Spread Function. I. A Semiempirical Method for Use in Natural Guide Star Observations," *PASP* **114**, pp. 1267–1280, Nov. 2002.

[33] E. Steinbring, S. M. Faber, B. A. Macintosh, D. Gavel, and E. L. Gates, "Characterizing the Adaptive Optics Off-Axis Point-Spread Function. II. Methods for Use in Laser Guide Star Observations," *PASP* **117**, pp. 847–859, Aug. 2005.

[34] M. Aubailly, *Reconstruction of anisoplanatic adaptive optics images.* PhD thesis, Michigan Technological University, 2005.

[35] C. D. Sheehy, N. McCrady, and J. R. Graham, "Constraining the Adaptive Optics Point-Spread Function in Crowded Fields: Measuring Photometric Aperture Corrections," *ApJ* **647**, pp. 1517–1530, Aug. 2006.

[36] M. C. Britton, "Analysis of crowded field adaptive optics image data," in *Advances in Adaptive Optics II. Edited by Ellerbroek, Brent L.; Bonaccini Calia, Domenico. Proceedings of the SPIE, Volume 6272, pp. (2006).*, July 2006.

[37] S. M. Jefferies and J. C. Christou, "Restoration of Astronomical Images by Iterative Blind Deconvolution," *ApJ* **415**, pp. 862–+, Oct. 1993.

[38] J. C. Christou, D. Bonnacini, N. Ageorges, and F. Marchis, "Myopic deconvolution of Adaptive Optics Images," *The Messenger* **97**, pp. 14–22, Sept. 1999.

[39] T. Fusco, J.-P. Véran, J.-M. Conan, and L. M. Mugnier, "Myopic deconvolution method for adaptive optics images of stellar fields," *A&A SS* **134**, pp. 193–200, Jan. 1999.

[40] T. Fusco, L. M. Mugnier, J.-M. Conan, F. Marchis, G. Chauvin, G. Rousset, A.-M. Lagrange, D. Mouillet, and F. J. Roddier, "Deconvolution of astronomical images obtained from ground-based telescopes with adaptive optics," in *Adaptive Optical System Technologies II. Edited by Wizinowich, Peter L.; Bonaccini, Domenico. Proceedings of the SPIE, Volume 4839, pp. 1065-1075 (2003).*, P. L. Wizinowich and D. Bonaccini, eds., pp. 1065–1075, Feb. 2003.

[41] L. M. Mugnier, T. Fusco, and J. M. Conan, "MISTRAL: a myopic edge-preserving image restoration method, with application to astronomical adaptive-optics-corrected long-exposure images,"

[42] F. Marchis, D. Le Mignant, F. H. Chaffee, A. G. Davies, S. H. Kwok, R. Prangé, I. de Pater, P. Amico, R. Campbell, T. Fusco, R. W. Goodrich, and A. Conrad, "Keck AO survey of Io global volcanic activity between 2 and 5 μm," *Icarus* **176**, pp. 96–122, July 2005.

[43] J. D. Drummond, "Adaptive optics Lorentzian point spread function," in *Proc. SPIE Vol. 3353, p. 1030-1037, Adaptive Optical System Technologies, Domenico Bonaccini; Robert K. Tyson; Eds.*, D. Bonaccini and R. K. Tyson, eds., pp. 1030–1037, Sept. 1998.

[44] D. Barnaby, E. Spillar, J. C. Christou, and J. D. Drummond, "Measurements of Binary Stars with the Starfire Optical Range Adaptive Optics Systems," *AJ* **119**, pp. 378–389, Jan. 2000.

[45] E. Diolaiti, O. Bendinelli, D. Bonaccini, L. M. Close, D. G. Currie, and G. Parmeggiani, "StarFinder: an IDL GUI-based code to analyze crowded fields with isoplanatic correcting PSF fitting," in *Proc. SPIE Vol. 4007, p. 879-888, Adaptive Optical Systems Technology, Peter L. Wizinowich; Ed.*, P. L. Wizinowich, ed., pp. 879–888, July 2000.